Studies of Relativistic Backward-Wave Oscillator Operation in the Cross-Excitation Regime

Frank Hegeler, *Member, IEEE*, Michael D. Partridge, *Student Member, IEEE*, Edl Schamiloglu, *Senior Member, IEEE*, and Chaouki T. Abdallah, *Senior Member, IEEE*

Abstract—We first reported the operation of a relativistic backward-wave oscillator (BWO) in the so-called cross-excitation regime in 1998. This instability, whose general properties were predicted earlier through numerical studies, resulted from the use of a particularly shallow rippled-wall waveguide [slow wave structure (SWS)] that was installed in an experiment to diagnose pulse shortening in a long-pulse electron beam-driven high-power microwave (HPM) source. This SWS was necessary to accommodate laser interferometry measurements along the SWS during the course of microwave generation. Since those early experiments, we have studied this regime in greater detail using two different SWS lengths. We have invoked time-frequency analysis, the smoothed-pseudo Wigner–Ville distribution in particular, to interpret the heterodyned signals of the radiated power measurements. These recent results are consistent with earlier theoretical predictions for the onset and voltage scaling for this instability. This paper presents data for a relativistic BWO operating in the single-frequency regime for two axial modes, operating in the cross-excitation regime, and discusses the interpretation of the data, as well as the methodology used for its analysis. Although operation in the cross-excitation regime is typically avoided due to its poorer efficiency, it may prove useful for future HPM effects studies.

Index Terms—Cross-excitation instability, high power microwaves, joint time-frequency analysis, mode competition, relativistic BWO.

I. INTRODUCTION

SINCE THE 1970's [1] there has been growing interest in the development of high-peak power microwave (HPM) devices driven by intensive relativistic electron beams, beginning with the backward wave oscillator (BWO). Kurilko *et al.* [2] presented the first comprehensive theoretical analysis describing the operation of an intense relativistic electron beam-driven BWO that was later expanded by Swegle and colleagues [3], [4]. Recently, Levush *et al.* [5] developed a theory of BWO operation that incorporates finite-length effects of the slow wave structure (SWS), in particular the effects of reflections of the microwaves at both ends of the device. Subsequent experiments and electromagnetic particle-in-cell (PIC) simulations by Moreland *et al.* [6] elucidated the role of finite length effects on both

microwave frequency and generation efficiency. In their work, Moreland *et al.* noted that a phase shift between the first and zeroth spatial harmonics plays a critical role in determining the operating characteristics of a finite-length BWO. Vlasov *et al.* [7] further studied this effect using a nonlinear model.

In their analysis, Levush *et al.* describe several operating regimes of intense relativistic electron beam-driven BWO's that strongly depend on the length of the beam–microwave interaction region (i.e., the number of ripple periods comprising the SWS) and the reflection coefficients at the ends. By sufficiently varying either the reflection coefficients or the beam parameters, mode competition can occur whereby two frequencies can be generated simultaneously. In particular, three parameters are considered in detail: a normalized length k_*L, the ratio of the beam current to start-oscillation current $\chi = I_{\text{beam}}/I_{st}$, and the reflection coefficient R at the downstream end of the SWS (the reflection coefficient at the upstream end is assumed to be 1.0 at the cutoff waveguide inlet to the electrodynamic system). Regarding the normalized length, k_* is the resonant wavenumber, defined by the intersection of the Doppler line with the cold SWS dispersion curve, and L is the physical length of the SWS. For a fixed-length SWS, the normalized length can still vary through changes in beam energy (caused in turn by changes in diode voltage) that will affect k_*. Fig. 1 shows the dispersion relation of the UNM long pulse BWO with a uniform SWS at the TM_{01} mode. As the beam voltage decreases, the resonant wavenumber k_* increases in order to preserve the intersection of the beam structure dispersion relation.

The value of k_* determines whether the BWO operates in a steady, single frequency regime or in a multifrequency regime characterized by instabilities that result from over-bunching of the electron beam (see Fig. 2). An additional regime exists where the start current and gain of one mode is modified by the presence of another saturated mode, enabling the second mode to compete with the first. Levush *et al.* refer to this regime as the "cross-excitation instability" regime. If the amplitudes of the two modes are approximately the same, the total power output and efficiency of the BWO are essentially unchanged, but no single-frequency equilibrium is achieved. If the second mode has a considerably larger amplitude, the first mode will be suppressed and a noticeable jump in efficiency, power output, and frequency will occur as the second mode reaches saturation. (The nonlinear excitation of parasitic modes in the context of gyrotrons was discussed by Nusinovich [8], and the essence of the cross-excitation instability can be understood in the context of the framework he describes.)
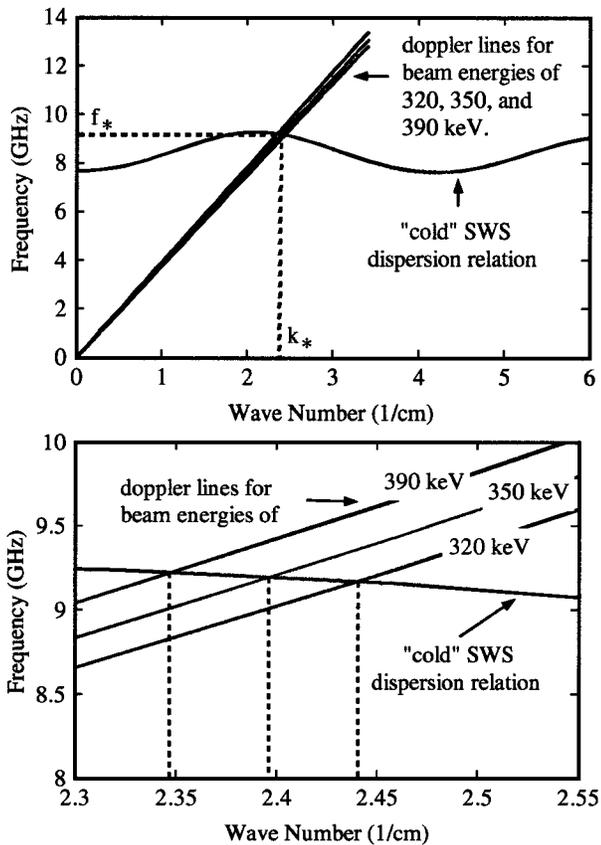
Fig. 1. The "cold" SWS dispersion relation of the UNM long pulse BWO at the TM_{01} mode. The resonant wavenumber k_* is defined by the intersection of the Doppler line with the cold SWS dispersion curve. (top) General overview. (bottom) Zoomed-in view of the SWS dispersion relation.

This paper describes the experimental observation of a long-pulse relativistic BWO operating in the single-frequency regime at two different axial modes, as well as it sweeping through the cross-excitation regime. The cross-excitation instability was alluded to as one of several mechanisms that could explain a frequency change during a power dip in an earlier BWO experiment [9], resulting in pulse shortening. The first observation of this instability where the appropriate scaling was demonstrated was reported by us in [10]. Since then, significant progress has been made in both the analysis of the measurements and in controlably operating in and out of this regime. Time-frequency analysis has proven to be invaluable in characterizing operation in the cross-excitation regime, both for a 10- and 12-period SWS. The remainder of this paper is organized as follows. Section II describes the experimental setup for the high-power microwave source, including the SWS configuration, and the microwave power and frequency diagnostics. Section III introduces the joint time-frequency analysis (JTFA) used to interpret the experimental data. Section IV presents the data and Section V discusses the conclusions. In the Appendix, both the Wigner–Ville (WV) and the smoothed-pseudo-WV distributions are described in more detail.

II. EXPERIMENTAL SETUP

The studies reported in this paper were conducted using the University of New Mexico (UNM) long-pulse BWO
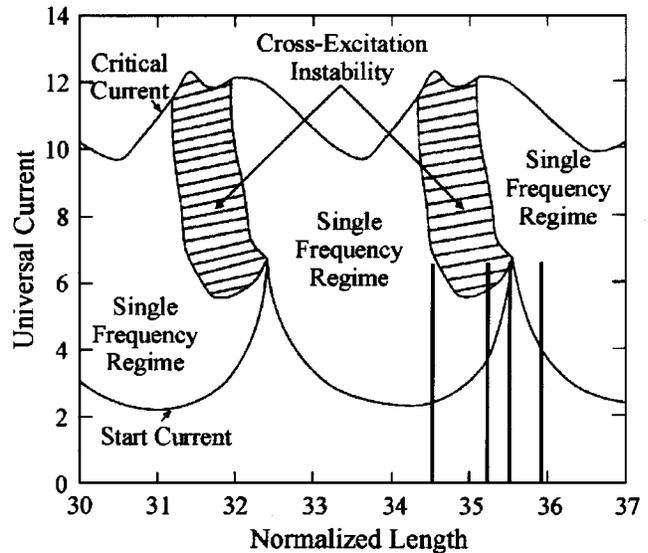

Fig. 2. Regions of BWO operation in the universal current-normalized length parameter space for a reflection coefficient of 0.7 at the downstream end of the SWS. The region of cross excitation will widen with a larger reflection coefficient. The vertical lines at the normalized lengths of 34.5, 35.2, 35.5, and 35.9 mark the positions of the experimental regimes with a 10-period SWS as shown as in Figs. 13, 9, 10, and 12, respectively. (The universal start current for this BWO can only be estimated, and thus, the exact value is unknown.) An overbunch instability regime exists in the area above the critical current.

experiment, shown schematically in Fig. 3. An electron beam is emitted from an annular knife-edge graphite cathode, and is guided by a magnetic field of 2 T through various SWS configurations onto a beam dump. All data presented in this paper have been obtained for peak cathode voltages ranging from 320 to 500 kV, beam currents ranging from 1 to 2 kA, and an anode-cathode (A–K) gap spacing of 2.5 cm. The generated microwaves are radiated using a conical horn antenna 12.7 cm in diameter, covered with a 0.25-mm-thick Mylar window to maintain the vacuum-to-air interface. (More complete information on the accelerator and the general experimental setup is available in [11].)

The SWS has a modular construction in which each ripple is machined out of a ring of stainless steel and then slid into a tube holding them in place. For operation in the cross-excitation regime, either a 10- or 12-period uniform amplitude structure was used, as shown in Fig. 4. This structure had been installed for a previous experiment to accommodate laser interferometry measurements during the course of microwave generation [12]. Each ring of the SWS has a width (ripple period) of 14.7 mm, a mean radius of 14.64 mm, and a ripple amplitude of 1.86 mm, and a minor inner diameter of 25.56 mm. The cutoff neck inlet to the electrodynamic structure has an inner diameter of 23 mm, and the annular electron beam is positioned between a radius of 9 mm and 11.5 mm [11]. (Note that the particularly shallow rippled-wall SWS is not optimized for maximum microwave generation efficiency.) The annual beam scrapes along the inner wall of the cutoff neck, producing plasma, which is one of the leading causes for pulse shortening. A detailed description of these measurements is given in [12]. Since this beam scraping occurs during operation in both the single-frequency and cross-
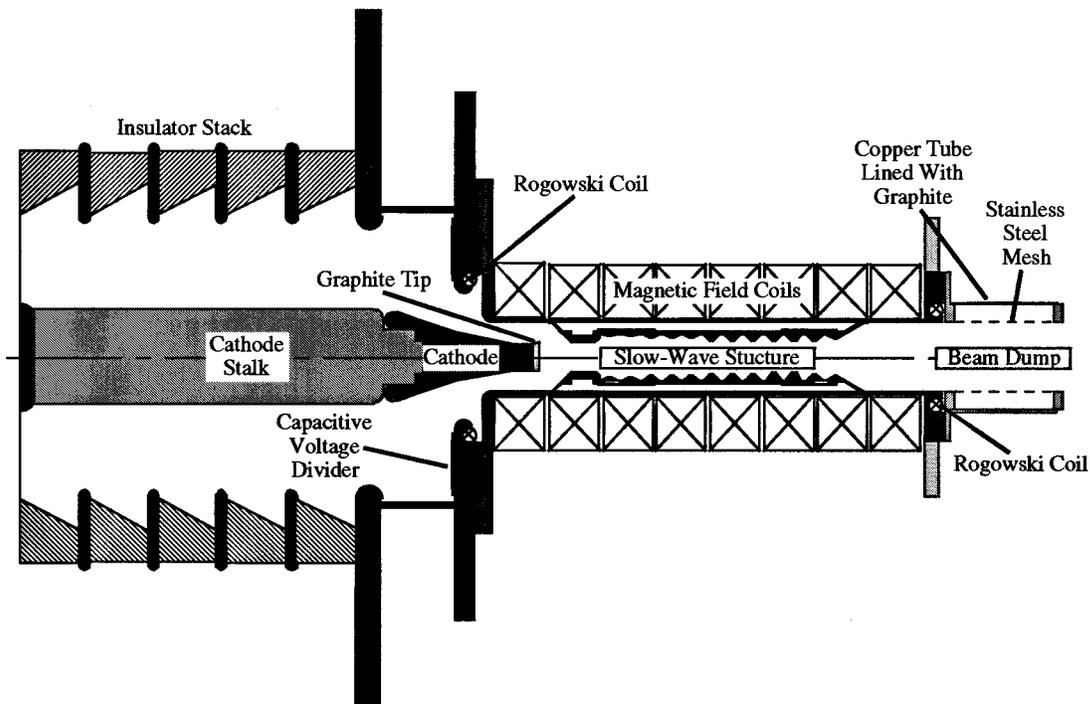
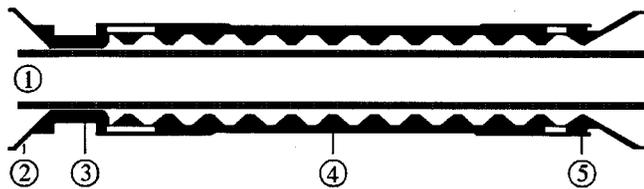Fig. 3. Cross-sectional diagram of the long-pulse BWO.

Fig. 4. Configuration of the uniform slow-wave structure. 1) Electron beam. 2) Anode of the A–K gap. 3) Cutoff neck. 4) Periodic ripple structure. 5) Impedance matching ring.

excitation regimes, it is not responsible for the cross-excitation instability.

Fig. 5 presents the setup used for microwave power and frequency measurements. The detector antenna, a short, open-ended section of WR-90 waveguide, is placed in the far-field region of the TM_{01}-mode radiation pattern at an angle of 25° from the centerline of the conical horn antenna. The BWO radiates in the TM_{01} mode in both the single-frequency and cross-excitation regimes. A directional coupler, semirigid coaxial cable, and coaxial attenuators reduce the microwave signal received by the detector antenna. The signal from the detector antenna is split into two signals using a power divider, one path that enters a crystal detector for power measurement, and the other heterodyned with a known local oscillator (LO) signal for frequency determination. In order to determine the microwave frequency more precisely, initial frequency measurements were taken using various LO frequencies. The attenuation of the microwave diagnostic components were calibrated using an HP8720D network analyzer, and the measurements are transferred to a personal computer using LabVIEW, taking into account the different attenuation values for various frequencies. Waveforms of the cathode voltage
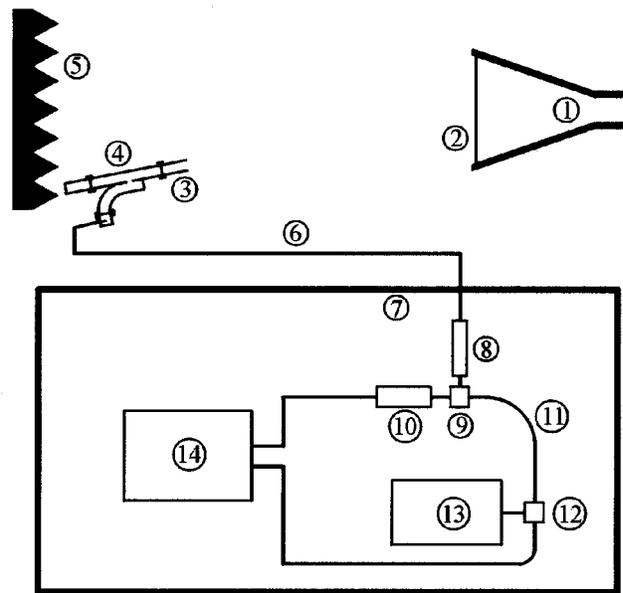

Fig. 5. Microwave power and frequency diagnostic setup for both the single frequency and cross-excitation regime. 1) Conical horn antenna. 2) 0.25-mm-thick Mylar window. 3) Open-ended x-band waveguide section. 4) 20-dB directional coupler, with termination and X-band to coaxial adapter. 5) Microwave absorbing material. 6) 17 m of RG402/U (EZ141) semirigid coaxial cable. 7) Shielded measurement room. 8) dc to 12.4 GHz attenuators. 9) 6-dB power splitter. 10) 0.01 to 18 GHz crystal detector. 11) 0.4 m of RG402/U (EZ141) semirigid coaxial cable. 12) 8–12 GHz double-balanced mixer. 13) Local oscillator. 14) Four-channel oscilloscope with a bandwidth of 1 GHz.

and beam current during microwave generation are presented in Fig. 6 for both the single-frequency and cross-exatation regimes, respectively. Microwaves are generated during the rising part of the voltage pulse, thus, for the calculation of
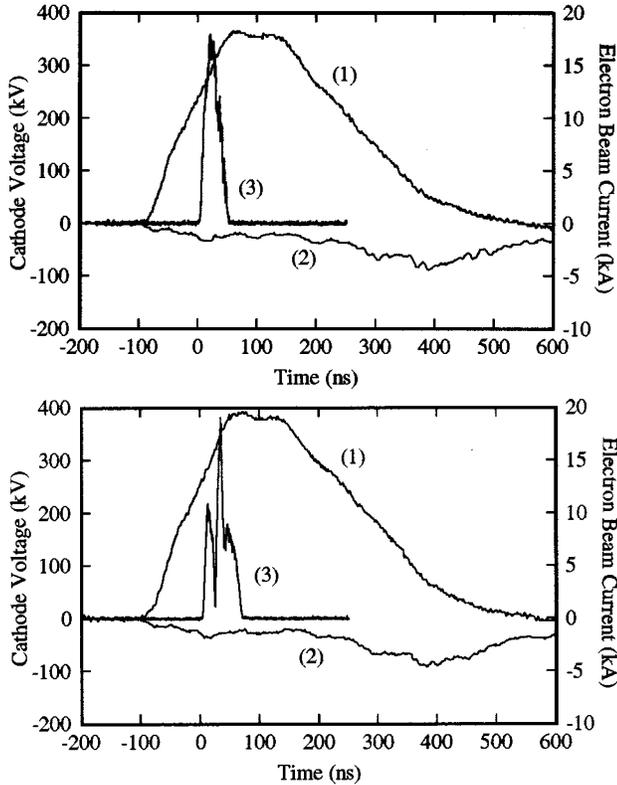
Fig. 6. Waveforms of the cathode voltage and beam current, overlaid with the microwave pulse. (top) BWO operation in a single-frequency mode. (bottom) Cross-excitation regime. The waveforms are obtained with a 10-period SWS. 1) Cathode voltage. 2) Electron beam current. 3) Microwave pulse.

the resonant wavenumber, k_* (see Fig. 1) the beam voltage is averaged for the duration of the microwave pulse. The current and voltage pulse shape presented in Fig. 6 are comparable in both the single-frequency and cross-excitation cases, except for the amplitudes of the voltage and current pulse. The microwave pulse starts at $t = 0$, for a duration of 50–70 ns, while the beam voltage rises at a rate of 2.3 kV/ns. Unlike in gyrotrons, where the output mode is extremely sensitive to the beam voltage, the frequency output of an intense beam BWO is only slightly dependent on the voltage amplitude. An increase of the A–K gap voltage leads to a rise in the beam current amplitude that will also increase the space charge in the beam. Although a larger beam voltage tends to increase the microwave frequency, the larger space charge counteracts this; thus, only a modest increase of the microwave frequency is observed. In fact, the drift in the frequency as a function in time can be attributed to the time-dependent change in voltage and current. Note that the two axial modes have been observed only when the shallow uniform ripple amplitude SWS is used. Other deeper ripple amplitude SWS's operate only in the single-frequency mode, even for cases where the cathode voltage rises at rates of 3 kV/ns.

III. JOINT TIME-FREQUENCY ANALYSIS APPLIED TO THE CROSS-EXCITATION REGIME

In previous frequency measurements, the heterodyned signal was separated into 10 segments, and a simple Fourier transform

of each segment was used to identify the major frequency components. Although this technique identifies frequency changes over the entire microwave signal, it loses the time information within the segment (or time window). In single-frequency operation, this not a concern. However, if there is a significant change in the microwave frequency, this loss of time information can lead to a misinterpretation of the data. Therefore, JTFA is used to better understand the frequency signal. The use of JTFA in the HPM community was first suggested by a group at the Israel Institute of Technology, Haifa, [13] and independently by a group at the University of Michigan [14]. We have tested various distributions for the JTFA to accurately display the temporal frequency measurements of the cross-excitation regime, which is the competition between (simultaneous presence of) two axial TM_{01} modes. The data presented in the next section are analyzed with a smoothed-pseudo WV (SPWV) distribution that is described in the Appendix.

IV. RESULTS AND DISCUSSION

Although the beam voltage increases over the course of the microwave pulse, as discussed in Section II, the BWO clearly sweeps through the cross-excitation regime since 1) the shape of the beam voltage is identical for the single-mode and cross-excitation regimes; 2) the cross-excitation instability is accessible only with the unique SWS as described in Section II—it is a consequence of the fact that the beam-to-start current ratio is slightly above unity. Other deeper ripple amplitude uniform SWS's do not show this kind of behavior since the start current is significantly lower (see Fig. 2) for the same time-dependent voltage behavior; 3) the JTFA of the microwave frequency signal does not necessarily show a frequency overlap for the case of mode hopping due to a beam voltage change; and 4) a large variation of the BWO beam voltage generates only a gradual drift in frequency. The data and discussion presented below are based on a series of approximately 100 shots taken with a 10- and 12-period uniform amplitude SWS at various beam voltages and currents. Out of these measurements, about 40 shots showed evidence of operation in the cross-excitation regime. Fig. 7 presents data representative of operation in the cross-excitation regime for the 12-period SWS. The experimental parameters of this shot are a peak diode voltage ($V_{\mathrm{diode,\,pk}}$) at the time of microwave generation of 400 kV and an average beam current ($I_{\mathrm{beam,\,avg}}$) of 1.8 kA. The normalized length for this case is $k_*L = 41.3$. Note that microwaves are produced on the rising edge of the UNM long-pulse accelerator voltage, whereas the diode voltage at the start of the microwave pulse is approximately 90% of $V_{\mathrm{diode,\,pk}}$. As can been seen from Fig. 7, the radiated power initially rises to 22 MW at an output frequency of about 9.1 GHz. Approximately 5 ns after the peak power is reached, the power rapidly decreases as the second axial mode within the SWS begins to grow. It is observed that two modes beat simultaneously for a period of 5 ns, after which point the highest radiated power occurs at a frequency of about 9.5 GHz. This second mode results in a considerably more efficient beam-to-microwave energy conversion. Note that in all cross-excitation results the frequency of the initial mode
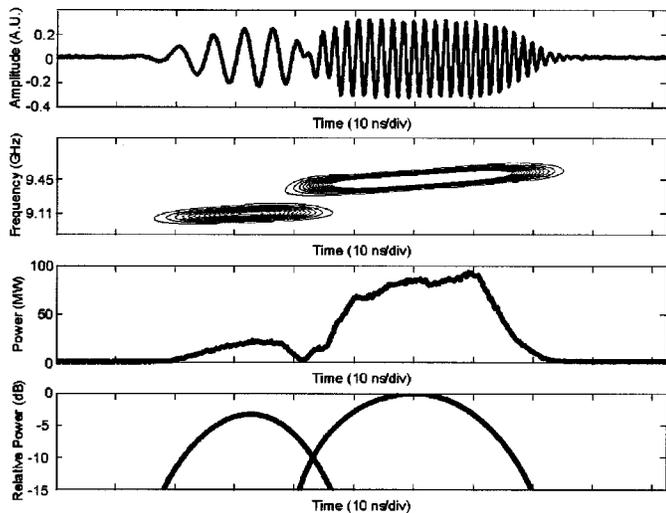
Fig. 7. Evidence of the cross-excitation instability. Top: Heterodyned frequency signal with a LO frequency of 8.9 GHz. Second from top: SPWV time-frequency distribution. Second from bottom: Microwave power. Bottom: Relative power in dB at the two mean frequencies of 9.11 and 9.45 GHz. ($V_{\mathrm{diode, pk}} = 400$ kV, $I_{\mathrm{b, avg}} = 1.8$ kA, and $k_* L = 41.3$, using a 12-period SWS.)

Fig. 9. Cross-excitation instability measured with a 10-period SWS. Top: Heterodyned frequency signal with a LO frequency of 9 GHz. Middle: SPWV time-frequency distribution. Bottom: Relative power in dB at the two mean frequencies of 9.21 and 9.57 GHz. ($V_{\mathrm{diode, pk}} = 350$ kV, $I_{\mathrm{b, avg}} = 1.2$ kA, and $k_* L = 35.2$.)
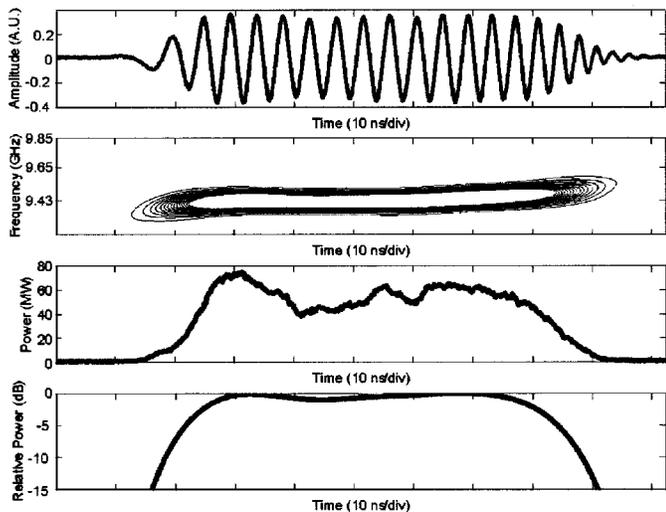

Fig. 8. Data illustrating single mode operation. Top: Heterodyned frequency signal with a LO frequency of 8.9 GHz. Second from top: SPWV time-frequency distribution. Second from bottom: Microwave power. Bottom: Relative power in dB at the mean frequency of 9.43 GHz. ($V_{\mathrm{diode, pk}} = 350$ kV, $I_{\mathrm{b, avg}} = 1.2$ kA, and $k_* L = 42.3$, using a 12-period SWS.)

Fig. 10. Cross-excitation instability measured with a 10-period SWS. Top: Heterodyned frequency signal with a LO frequency of 9 GHz. Middle: SPWV time-frequency distribution. Bottom: Relative power in dB at the two mean frequencies of 9.05 and 9.41 GHz. ($V_{\mathrm{diode, pk}} = 340$ kV, $I_{\mathrm{b, avg}} = 1.2$ kA, and $k_* L = 35.5$.)

is lower than the frequency of the second mode, since the diode voltage increases during the duration of the microwave pulse.

When the diode voltage is decreased to 350 kV, which also decreases the beam current to 1.2 kA, the normalized length $k_* L$ is shifted to 42.3, and the ratio of the beam current to start-os-cillation current χ is reduced compared to the previous case. In this single-frequency regime (see Fig. 8), the frequency varies slightly from 9.43–9.5 GHz owing to an increase of the diode voltage during microwave generation. The maximum radiated power is less than the data shown in Fig. 7 since the beam energy is reduced. In addition, it is evident from Figs. 7 and 8 that the maximum beam-to-microwave energy conversion efficiency
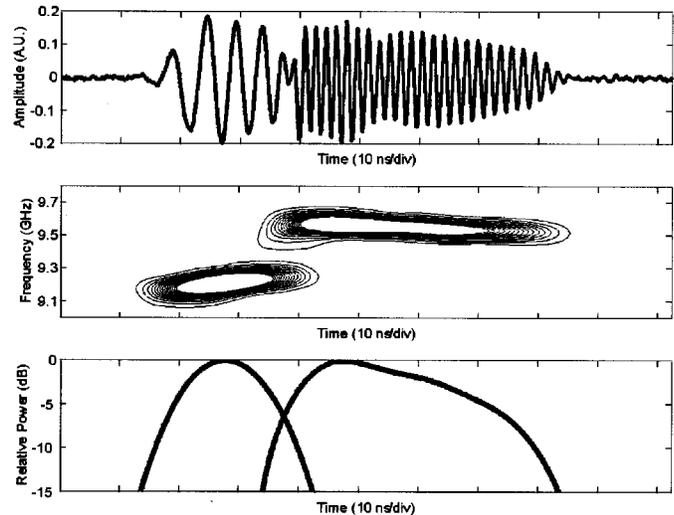
in single-mode operation is greater than in the cross-excitation regime.

Operation in the cross-excitation regime is also observed when the BWO is fitted with a shorter SWS that consists of 10 periods. Figs. 9–11 present a variety of data with similar normalized lengths $k_* L$ of 35.2–35.5. With slight variations of the beam voltage and current parameters, large changes in the operation in the cross-excitation regime are evident. Fig. 9 presents data in the cross-excitation regime where the two axial modes have similar maximum power levels. Fig. 10 presents data in the cross-excitation regime where the initial axial mode has a lower power level compared with the second axial mode, and Fig. 11 illustrates the opposite case.
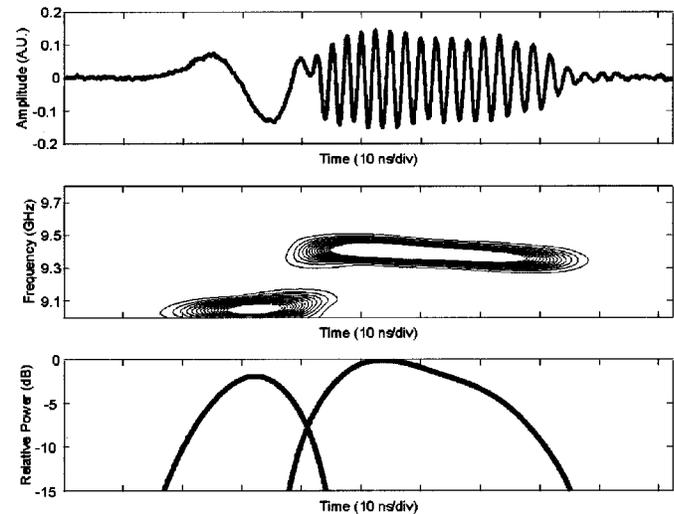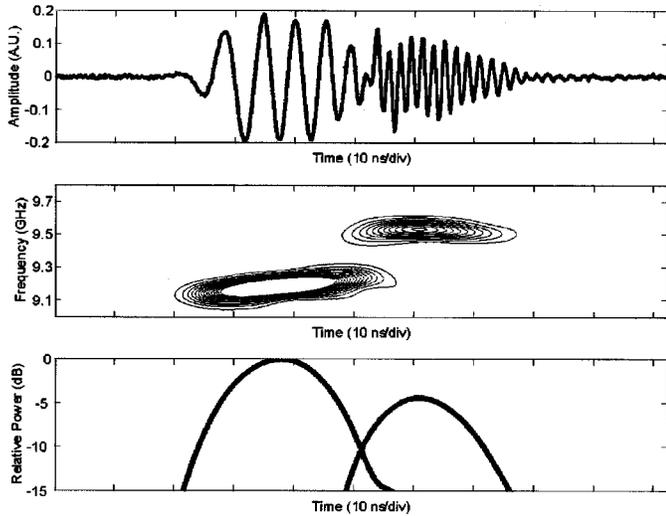
Fig. 11. Cross-excitation instability measured with a 10-period SWS. Top: Heterodyned frequency signal with a LO frequency of 9 GHz. Middle: SPWV time-frequency distribution. Bottom: Relative power in dB at the two mean frequencies of 9.19 and 9.54 GHz. ($V_{\mathrm{diode,pk}} = 340$ kV, $I_{\mathrm{b,avg}} = 1.1$ kA, and $k_* L = 35.5$.)
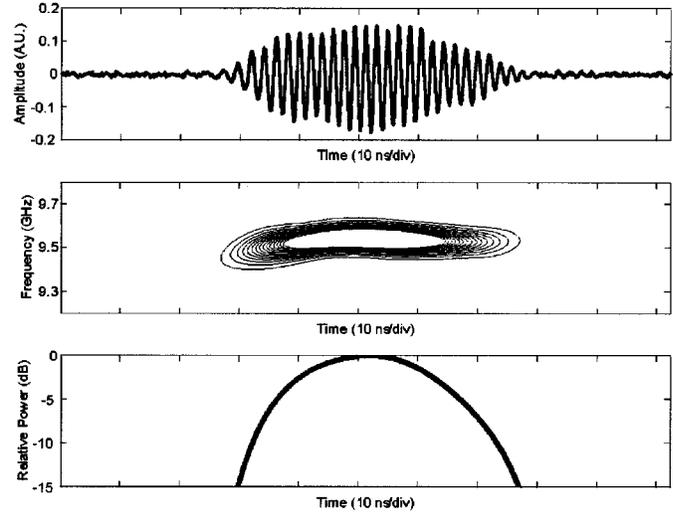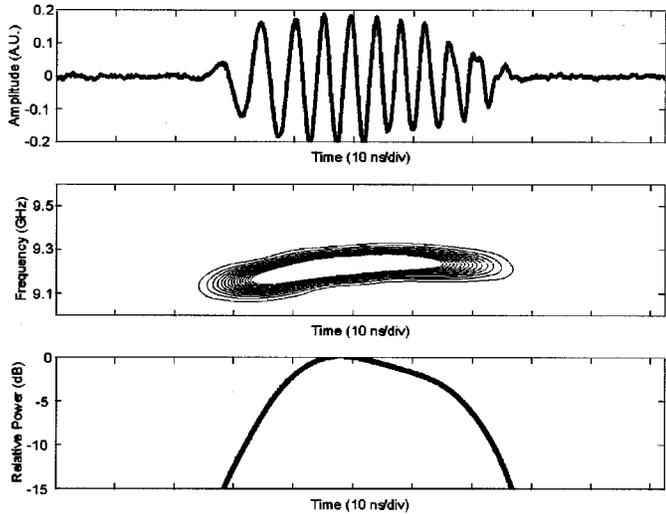

Fig. 13. High-frequency single-mode operation measured with a 10-period SWS. Top: Heterodyned frequency signal with a LO frequency of 9 GHz. Middle: SPWV time-frequency distribution. Bottom: Relative power in dB at the mean frequency of 9.5 GHz. ($V_{\mathrm{diode,pk}} = 390$ kV, $I_{\mathrm{b,avg}} = 1.7$ kA, and $k_* L = 34.5$.)

the cross-excitation regime is equal to or slightly larger than for the case with a single frequency. Since the power amplitude decreases during the simultaneous beating of the two axial modes in the cross-excitation regime, the microwave energy for the single frequency case is greater.

V. CONCLUSION

We have presented data where an intense relativistic electron beam-driven BWO operates in the single-frequency regime at one of two neighboring axial modes, and we have demonstrated how slight changes in the beam parameters can lead to operation in the cross-excitation regime, where the onset of one mode non-linearly decreases the start conditions for a neighboring mode, and mode competition results. The scaling of this behavior is consistent with nonlinear simulations presented earlier, and the observations support the validity of those models. Time-frequency analysis was used to interpret the frequency output of the source, and was critical to identifying the coexistence in time between the two axial modes. This is a rich area of non-linear physics that needs to be further explored. Future work will study the factors that contribute to the temporal coexistence of the modes, yielding some insight into mode saturation and/or electron trapping. Although operation in the cross-excitation regime is less efficient that single-frequency operation, it may prove useful to future HPM effects studies.

APPENDIX I

For the JTFA we explored several methods, such as wavelets, smoothed-pseudo-Wigner–Ville distributions, spectrograms, and Gabor distributions [15]–[24]. These distributions were selected based upon their ability to discriminate frequency overlap in time. Each of the JTFA techniques was evaluated with "artificial data" that was generated from two single-frequency signals. By "artificial data" we mean analytic signals that were generated numerically and looked similar to the

Fig. 12. Low-frequency single-mode operation measured with a 10-period SWS. Top: Heterodyned frequency signal with a LO frequency of 9 GHz. Middle: SPWV time-frequency distribution. Bottom: Relative power in dB at the mean frequency of 9.2 GHz. ($V_{\mathrm{diode,pk}} = 320$ kV, $I_{\mathrm{b,avg}} = 1.0$ kA, and $k_* L = 35.9$.)

Although the universal start current for this BWO can only be estimated, and thus, a direct comparison with the original modeling results is not possible, the experimental data for the 10-period SWS at the normalized lengths $k_* L$ are consistent with the position of the cross-excitation instability region (see Fig. 2). Single-mode operation with the 10-period SWS is obtained when the diode voltage is either decreased or increased compared to the value of $V_{\mathrm{diode,pk}}$ corresponding to operation in the cross-excitation regime. Lowering the diode voltage will lead to single-frequency operation at the lower axial mode (see Fig. 12), and increasing the diode voltage will lead to single-frequency operation at the higher axial mode (see Fig. 13). Pulse shortening due to cross excitation has not been observed. On average, the microwave pulse duration in

Fig. 14. Artificial data used for calibration of the JTFA. Top: "Heterodyned" frequencies of 100 MHz and 450 MHz with no overlap and a local oscillator frequency of 9 GHz. Middle: SPWV time-frequency distribution. Bottom: Relative power in dB at the two mean instantaneous frequencies of 9.1 and 9.45 GHz.
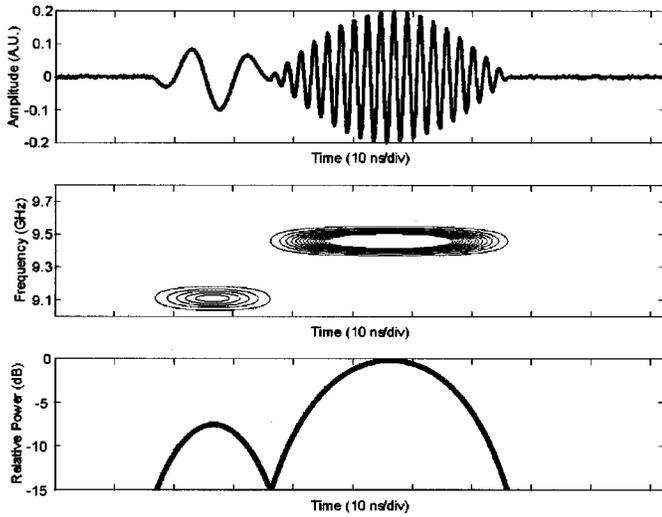

Fig. 15. Artificial data used for calibration of the JTFA. Top: "Heterodyned" frequencies of 100 MHz and 450 MHz with a 5 ns overlap and a local oscillator frequency of 9 GHz. Middle: SPWV time-frequency distribution. Bottom: Relative power in dB at the two mean instantaneous frequencies of 9.1 and 9.45 GHz.

experimentally obtained heterodyned signals. At the beginning and end of the artificial data, a low-amplitude random signal was added to simulate measurement noise, and each frequency signal was amplitude modulated with a cosine distribution. Using the various JTFA techniques described above to analyze the artificial data with a known frequency overlap in time, the WV distribution yielded the most accurate representation of the overlap in energy content of the signals. For a clearer representation of the frequency overlap, the interference terms from the time-frequency distribution were eliminated using a SPWV distribution. The time smoothing carried out by the SPWV reduces the interference terms, but also decreases the time-frequency resolution. The most accurate analysis of the artificial data without interference terms from the JTFA was obtained using a sinusoidal window of 79 points (with 5 points equaling 1 ns) for time smoothing, and a Gaussian window of 79 points for frequency smoothing. Figs. 14 and 15 show the results of the JTFA with a SPWV distribution for 0 ns and 5 ns overlap, respectively. The relative power plots in Figs. 14 and 15 explicitly indicate the amount of time that the two axial modes coexist. (A LO frequency of 9.0 GHz was used in the artificially generated data.) Since the data in these two figures is artificially generated, we do not display an overall power envelope. Similar figures are presented in the results and discussion section that show the relative power plots in addition to the overall measured power envelope. Since the relative power plots are expressed in dB and track the power content for a fixed frequency, there may be little resemblance between the relative power plot and the overall power envelope.

The analytic single used in this analysis $x_a(t)$ is given by

$$x_a(t) = x(t) + jHT[x(t)] \tag{A1}$$

where HT is the Hilbert transform of $x(t)$. This transformation will remove the negative frequency values and double the pos-

itive ones when a Fourier transform of $x(t)$ is taken. The WV distribution is defined as

$$W_x(t, \nu) = \int_{-\infty}^{+\infty} x\left(t + \frac{\tau}{2}\right) x^*\left(t - \frac{\tau}{2}\right) e^{-j2\pi\nu t}\, d\tau. \tag{A2}$$

However, many interference terms are present due to the bilinearity of the WV distribution. Two points of the time-frequency distribution interfere with each other and create a third point, at a frequency that is proportional to the distance between these points. The interference terms are shown in the following equation:

$$W_{x+y}(t, \nu) = W_x(t, \nu) + W_y(t, \nu) + 2\text{Re}[W_{x,y}(t, \nu)] \tag{A3}$$

where the interference term, $W_{x,y}$ is defined by

$$W_{x,y}(t, \nu) = \int_{-\infty}^{+\infty} x\left(t + \frac{\tau}{2}\right) y^*\left(t - \frac{\tau}{2}\right) e^{-j2\pi\nu t}\, d\tau. \tag{A4}$$

For a clearer representation of the frequency overlap, the SPWV distribution is used:

$$\text{SPWV}_x(t, \nu) = \int_{-\infty}^{+\infty} h(\tau) \int_{-\infty}^{+\infty} g(s - t) x\left(s + \frac{\tau}{2}\right)$$
$$\cdot x^*\left(s - \frac{\tau}{2}\right) e^{-j2\pi\nu t}\, ds\, d\tau \tag{A5}$$

where $h(t)$ is the frequency-smoothing window and $g(t)$ is the time-smoothing window.

Several sinusoidal and Gaussian-based frequency-smoothing and time-smoothing windows have been evaluated for the SPWV distribution. All the SPWVs described in this paper use a sinusoidal window for time-smoothing and a Gaussian window for frequency smoothing, each with the same window
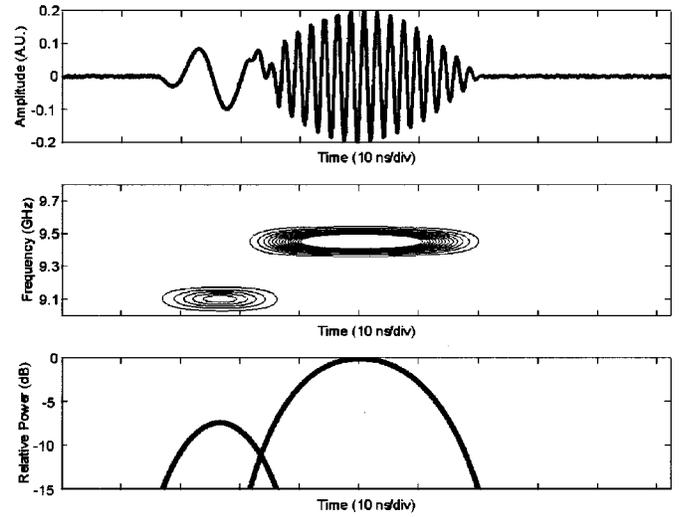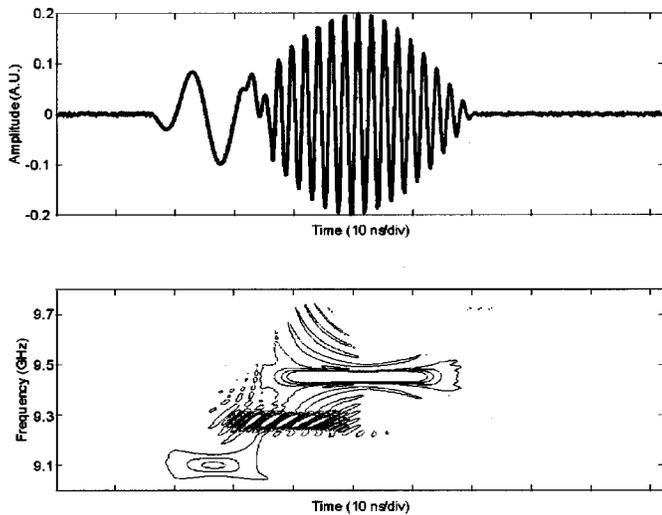
Fig. 16.   Artificial data used for calibration of the JTFA. Top: "Heterodyned" frequencies of 100 MHz and 450 MHz with a 5 ns overlap and a local oscillator frequency of 9 GHz. Bottom: WV time-frequency distribution with interference terms.

width of 79 points. (Note that SPWV results for sinusoidal and Gaussian-based time-smoothing windows are very similar.)

An example of the WV distribution with interference terms is shown in Fig. 16. The artificial frequency data used in this figure is identical to the one of Fig. 15. Although the WV distribution shows the same mean instantaneous frequencies of 9.1 and 9.45 GHz as the SPWV distribution, the overlap region of both frequency signals is not observable due to the interference terms.

REFERENCES

[1] J. A. Nation, "On the coupling of an high-current relativistic electron beam to a slow wave structure," *Appl. Phys. Lett.*, vol. 17, pp. 491–494, 1970.
[2] V. I. Kurilko, V. I. Kucherov, A. D. Ostrovskii, and Yu. V. Thach, "Stability of a relativistic electron beam in a periodic cylindrical waveguide," *Sov. Phys. Tech. Phys.*, vol. 24, pp. 1451–1454, 1979.
[3] J. A. Swegle, J. W. Poukey, and G. T. Leifeste, "Backward-wave oscillators with rippled wall resonators: Analytic theory and numerical-simulation," *Phys. Fluids*, vol. 28, pp. 2882–2894, 1985.
[4] J. A. Swegle, "Approximate treatment near resonance of backward and traveling wave tubes in the compton regime," *Phys. Fluids*, vol. 28, pp. 3696–3702, 1985.
[5] B. Levush, T. M. Antonsen Jr., A. Bromborsky, W. R. Lou, and Y. Carmel, "Theory of relativistic backward-wave oscillators with end reflections," *IEEE Trans. Plasma Sci.*, vol. 20, pp. 263–280, 1992.
[6] L. D. Moreland, E. Schamiloglu, R. W. Lemke, A. M. Roitman, S. D. Korovin, and V. V. Rostov, "Enhanced frequency agility of high-power relativistic backward wave oscillators," *IEEE Trans. Plasma Sci.*, vol. 24, pp. 852–858, 1996.
[7] A. N. Vlasov, G. S. Nusinovich, and B. Levush, "Effect of the zero spatial harmonic in a slow electromagnetic-wave on operation of relativistic backward-wave oscillators," *Phys. Plasmas*, vol. 4, pp. 1402–1412, 1997.
[8] G. S. Nusinovich, "Mode interaction in gyrotrons," *Int. J. Electron.*, vol. 51, pp. 457–474, 1981.
[9] J. A. Swegle, R. A. Anderson, J. F. Camacho, B. R. Poole, M. A. Rhodes, E. T. Rosenbury, and D. L. Shaeffer, "Scaling studies and time-resolved microwave measurements on a relativistic backward-wave oscillator," *IEEE Trans. Plasma Sci.*, vol. 21, pp. 714–724, 1993.
[10] C. Grabowski, E. Schamiloglu, C. T. Abdallah, and F. Hegeler, "Observation of the cross-excitation instability in a relativistic backward wave oscillator," *Phys. Plasmas*, vol. 5, pp. 3490–3492, 1998.
[11] C. Grabowski, J. M. Gahl, and E. Schamiloglu, "Electron-emission from slow-wave structure walls in a long-pulse, high-power backward-wave oscillator," *IEEE Trans. Plasma Sci.*, vol. 25, pp. 335–341, 1997.
[12] F. Hegeler, C. Grabowski, and E. Schamiloglu, "Electron density measurements during microwave generation in a high power backward wave oscillator," *IEEE Trans. Plasma Sci.*, vol. 26, pp. 275–281, 1998.
[13] I. Cohen, S. Raz, and D. Malah, "Time-frequency analysis and noise suppression with shift-invariant wavelet packets," in *Ultra-Wideband, Short Pulse Electromagnetics 4*, Heyman *et al.*, Eds. New York: Kluwer Academic/Plenum, 1999, pp. 401–408.
[14] C. W. Peters, R. L. Jaynes, Y. Y. Lau, R. M. Gilgenbach, W. J. Williams, J. M. Hochman, W. E. Cohen, J. I. Rintamaki, D. E. Vollers, and T. A. Spencer, "Time-frequency analysis of modulation of high-power microwaves by electron-beam voltage fluctuations," *Phys. Rev. E*, vol. 58, pp. 6880–6883, 1998.
[15] L. Cohen, "What is a multicomponent signal," in *Proc. IEEE Int. Conf. on Acoust., Speech Signal Processing (ICASSP-92)*, Mar. 1992, pp. 113–116.
[16] ——, *Time-Frequency Analysis*. New York: Prentice-Hall, 1995.
[17] B. Boashash, Ed., *Time-Frequency Signal Analysis*, Melbourne: Longman Chesire, 1992.
[18] S. Qian and D. Chen, "Joint time-frequency analysis," *IEEE Signal Processing Mag.*, vol. 16, pp. 52–67, 1999.
[19] S. Mallat, *A Wavelet Tour of Signal Processing*. New York: Academic, 1998.
[20] G. Strang and T. Nguyen, *Wavelets and Filter Banks*. Wellesley, MA: Wellesley-Cambridge, 1996.
[21] O. Rioul and M. Vetterli, "Wavelets and signal processing," *IEEE Signal Processing Mag.*, vol. 8, pp. 14–38, 1991.
[22] S. D. Meyers, B. G. Kelly, and J. J. O'Brien, "An introduction to wavelet analysis in oceanography and meterology," *Month. Weather Rev.*, vol. 121, pp. 2858–2866, 1993.
[23] I. Daubechies, *Ten Lectures on Wavelets*. New York: SIAM, 1992.
[24] F. Auger, P. Flandrin, P. Goncalves, and O. Lemoine, "Tutorial: Time-frequency toolbox for use with Matlab," Centre National de la Recherche Scientifique (CNRS) and Rice University, Available at http://crttsn.univ-nantes.fr/~auger/tftb.html, 1995–1996.

Frank Hegeler (S'91–M'95) was born in Oldenburg, Germany, in 1965. He received the Dipl.-Ing. degree in electrical engineering from Fachhochschule Wilhelmshaven in 1989, and the M.S.E.E. and Ph.D. degrees from Texas Tech University, Lubbock, in 1991 and 1995, respectively.

From June 1995 to March 1997, he was with the Department of Electrical and Computer Engineering, Kumamoto University, Japan, as a Visiting Associate Professor. He joined the Department of Electrical and Computer Engineering, University of New Mexico, Albuquerque, in 1997, and is presently a Research Assistant Professor. He has authored or coauthored 8 refereed journal and 24 conference papers, and an article on plasma switches for the *Wiley Encyclopedia of Electrical and Electronics Engineering*. His interests are plasma diagnostics, high-power microwave sources, nonthermal atmospheric-pressure plasma reactors, microwaves for wireless communication, dielectric surface breakdown, and basic and applied pulsed power.

Michael D. Partridge (S'99) received the B.S. degree in physics and the M.S. degree in electrical engineering from the University of New Mexico, Albuquerque, NM, in 1998 and 2000, respectively.

From 1996 to 1998, he worked as a Research Assistant with the University of New Mexico (UNM) Department of Physics and Astronomy developing nuclear medicine digital imaging equipment. In 1998, he also worked as a Teaching Assistant for the junior and senior physics laboratories at UNM. Since 1999, he has worked as a Research Assistant with the Department of Electrical and Computer Engineering, UNM Pulsed Power and Plasma Science Laboratory. His research interests are time-frequency analysis and broad-band wireless channel equalization. He is presently with Aerospace Corporation.

Edl Schamiloglu (M'90–SM'95) received the B.S. and M.S. degrees from the School of Engineering and Applied Science, Columbia University, New York, in 1979 and 1981, respectively. He received the Ph.D. degree in applied physics from Cornell University, in 1988.

He was appointed Assistant Professor of electrical and computer engineering, University of New Mexico (UNM) in 1988 and cofounded the Pulsed Power and Plasma Science Laboratory, which he presently directs. He is presently Gardner–Zemke Professor of electrical and computer engineering. In the summer of 1990 he was a Lecturer with the U.S. Particle Accelerator School (USPAS), Harvard University, and in the summer of 1997 he lectured at the USPAS at MIT. His research interests are in the physics and technology of charged particle-beam generation and propagation, high-power narrow-band and ultrawide-band microwave sources, plasma physics and diagnostics, and electromagnetic wave propagation.

Dr. Schamiloglu received the Sandia National Laboratories Research Excellence Award (1991), the UNM School of Engineering Research Excellence Award (1992), and the title of Regents' Lecturer (1996). He is a member of the American Physical Society and a member of the ASEE. He is an Associate Editor of the IEEE TRANSACTIONS ON PLASMA SCIENCE, an elected member of the Administrative Committee of the IEEE Nuclear and Plasma Sciences Society, and an elected member of the Executive Committee of the Plasma Sciences and Applications subcommittee of the IEEE Nuclear and Plasma Sciences Society. He is coeditor of a forthcoming book entitled *Advances in High Power Microwave Sources and Technologies* (IEEE Press: 2001) (with R. J. Barker), and he is coauthor of *High Power Microwaves,* 2nd ed. (Institute of Physics Publishing: 2002) (with J. Benford and J. Swegle). He has authored or coauthored 35 refereed journal and 46 reviewed conference papers, and serves on the international program committee of numerous conferences in pulsed power, plasma science, and high power microwave sources.

Chaouki Abdallah (SM'95) received the B.E. degree in electrical engineering in 1981 from Youngstown State University, Youngstown, OH, the M.S. degree in 1982, and the Ph.D. degree in electrical engineering in 1988 from Georgia Tech, Atlanta, GA.

Between 1983 and 1985, he was with SAWTEK Inc., Orlando, FL, where he designed RF components and systems for signal processing and communications engineering. He joined the Department of Electrical and Computer Engineering at the University of New Mexico, Albuquerque, NM in 1988 and was promoted to Associate Professor in August 1994. He has taught courses in control theory, wireless communications, and neural networks. He was Exhibit Chairman of the 1990 International Conference on Acoustics, Speech, and Signal Processing (ICASSP) and the local arrangements chairman for the 1997 American Control Conference. He is currently serving as the Program Chair for the 2003 CDC. His research interests are in the areas of control and communications.

Dr. Abdallah is a co-editor of *Robot Control: Dynamics, Motion Planning, and Analysis* (IEEE Press) and coauthor of *Control of Robot Manipulators* and *Linear Quadratic Control: An Introduction* (Prentice-Hall).